J Solid State Electrochem (2008) 12:885–894
DOI 10.1007/s10008-007-0449-3

ORIGINAL PAPER

# Failure mechanism of Li-ion battery at overcharge conditions

**D. Belov · Mo-Hua Yang**

Received: 2 July 2007 / Revised: 1 October 2007 / Accepted: 10 October 2007 / Published online: 13 November 2007


**Abstract** The overcharge kinetics of a commercial prismatic Li-ion battery at different current rates (1 C, 2 C, and 3 C) has been studied. Battery surface temperature, heat output, and voltage were monitored and analyzed during overcharge testing. It has been shown that the heat rate of the battery surface does not increase in proportion to the applied current rate. Separator shutdown properties may be realized for heat rates less than 3 °C/min. Li-ion batteries have been submitted to different stages of overcharge by a "soft" overcharge technique (1 C to 4.4, 4.6, and 5.0 V). Differential scanning calorimetry (DSC) tests of the charged anode, cathode, and separator recovered from overcharged cells have been performed. It was found that the anode at different overcharged states has two main exothermic peaks at 120 and 300–320 °C. At a higher state of overcharge (SOOC), the second peak shifts to a lower temperature. DSC for overcharged cathodes has more complicated profiles depending on SOOC. Increasing the cutoff voltage from 4.4 to 5.0 V shifts the maximum of the first temperature peak from 235 to 200 °C and the second from 345 to 320 °C. Electrical impedance spectroscopy and scanning electron microscopy have been used to characterize electrode materials at different SOOC and overcharge conditions. The heat rate (related to current), cell construction, and design are considered as the main factors of Li-ion battery failure at overcharge.

Contribution to ICMAT 2007, Symposium K: Nanostructured and bulk materials for electrochemical power sources, July 1–6, 2007, Singapore.

D. Belov (✉) · M.-H. Yang
Material and Chemical Research Laboratories,
Industrial Technology Research Institute,
Hsinchu 31040, Taiwan
e-mail: dmitrybelov@itri.org.tw

**Keywords** Overcharge · Li-ion battery · Anode · Cathode · Separator

## Introduction

The most advanced chemistry for a Li-ion battery presently on the market is $Li_xCoO_2/Li_yC_6$ with $LiPF_6$ salt in non-aqueous electrolyte solvent. $LiCoO_2$ is considered to be the most unstable at abuse conditions compared to other types of cathode materials [1–3]. Safety problems for Li-ion batteries have existed for a decade (since it was introduced by Sony in the early 1990s) and the overcharge is one of them. Although overcharge for a single cell may not be as big a problem, a battery package (laptop, power tooling, light electric vehicle, etc.) has the potential to become a serious problem even with smart electronic circuit protection installed. However, the main factor(s) leading to cell failure at overcharge are still not clear. After reviewing many reports on Li-ion cell tests during abuse conditions such as overcharge, we found that most researchers agree that the main reason for such behavior is thermal and chemical instability of the layered cathode composites at certain discharge states. For example, the stability of $Li_xCoO_2$ is believed to be limited to $1<x<0.5$ [4]. Above some critical temperature, layered materials such as $Li_xNiO_2$ and $Li_xCoO_2$ become unstable and may liberate oxygen into the electrolyte which, when heated above its flash point, react violently [5]. The amount of released oxygen depends on $x$ and will increase with decreasing $x$ but it also depends on the crystal structure and particle size. Another source of heat generation in the Li-ion battery is the anode material (particle size, crystal structure, and porosity) and binder type and its amount [3].

Most of the described thermal reactions in Li-ion batteries (studied by differential scanning calorimetry (DSC) and accelerating rate calorimetry methods) start from 200 °C. These include thermal decomposition of the electrolyte with negative material, thermal decomposition of the positive material and reaction with electrolyte, and reaction of polyvinylidene difluoride (PVDF) binder with lithiated negative material (>300 °C). Only one exothermic reaction starts at 120 °C and is proposed to be solid electrolyte interface (SEI) layer breakdown. These thermal reactions are quite far from the onset point of battery thermal runaway, which starts at 80 °C (cell surface temperature). However, the real route for thermal runaway of a Li-ion battery may be more complicated and it is interconnected with many reactions for which priority may be varied (depending on active material nature, electrolyte composition including Li salt type, cell design, etc.).

According to the literature, most efforts in improving Li-ion battery safety at overcharge are directed to finding safer electrode materials ($LiFePO_4$) or improving thermal stability of the existing cathode material by coating the surface with additives [6–8]. Another direction is to use overcharge protection additives for electrolytes [9–11]. However, the test vehicle's type, i.e., cell design, in each study is different, e.g., coin cell, low-capacity pouch cell (300 mA h), winding- or stacking-type electrode, different electrolyte composition, salt concentration and its type, separator type polypropylene (PP), polyethylene (PE) or PP/PE/PP and its thickness, and so on. It is possible to see some safety improvements, however only in particular cases, which bring more illusion about safety improvement rather than real solution.

Over several years, standards for battery safety have been developed by Underwriters Laboratories Requirements [12], Technical Inspection Association, Japanese Industrial Standard [13], and many others. However, accidents involving Li-ion batteries still occur and are sometimes quite serious. The new safety guidelines developed by Japan Electronics and Informational Technology Industries Association released on April 20, 2007 (after Sony's recall of their laptop batteries) stressed the importance of avoiding high-speed charging using higher than rated voltages.

In this study, we trace the overcharge process step by step until cell explosion and ignition. Overcharge conditions used in this study (a) follow the standards for overcharge testing as well as customers requests and (b) the so-called "soft" overcharge which allows us to monitor and investigate cell parameters and material change for each stage of overcharge (from 4.2 to >5 V) before the cell is destroyed.

## Materials and methods

The commercial cell type chosen for this study is a prismatic Li-ion cell with 720-mA h nominal capacity (dimension is 40×34×50—thickness × width × height) in an Al can with safety pressure-release rupture and vent (specific energy 170 Wh/kg, energy density 375 Wh/l). The positive electrode material was $LiCoO_2$ (Seimi Chemical Co., Ltd., Japan, 12 μm in diameter) which consists of 90% $LiCoO_2$, 7% conducting carbon SuperP (EraChem, Baltimore, MD, USA), and 3% polyvinylidene difluoride (PVDF; Kureha, Japan) on aluminum foil (thickness—25 μm). The negative electrode material was mesocarbon microbeads (MCMB-2528; Osaka Gas Co. Ltd., Osaka, Japan) with 92% on copper foil (thickness—15 μm). The electrolyte contains ethylene carbonate (EC; boiling point (bp)=238 °C), propylene carbonate (bp=242 °C), and ethyl methyl carbonate (EMC; bp=108 °C; it should be noted that exact electrolyte composition is proprietary knowledge) with 1.1- and 1.25-M $LiPF_6$ (bp=200 °C; Mitsubishi Chem. Ltd., Tokyo, Japan). A PE separator E16MMS of thickness 16 μm (Tonen Corp, Japan) was used.

After assembly, cells were subjected to five formation cycles by charging and then discharging at a low rate (C/25) to form a smooth SEI layer on the electrode surface and slow gas generation by the electrolyte decomposition during SEI formation. For cell conditioning, a Toyo multichannel battery cycler (Japan) was used. After formation, cells were charged at the chosen current to a voltage limit of 4.2 V, followed by holding at 4.2 V until the current dropped below C/20 or for a maximum of 2 h. The discharging was constant where the current was set to a voltage of 2.8. This procedure is considered to be 100% depth of discharge.

Impedance studies of the cells before and after overcharge testing were carried out with the AutoLab Instrument Frequency Response Analyzer (FRA) and a potentiostat (The Netherlands) and analyzed with FRA software (AutoLab).

A DSC test of positive and negative electrodes before and after overcharge testing was performed in aluminum containers with a Pyris 6 DSC (Perkin–Elmer) in the temperature range 40–300 °C. Electrode samples were obtained from fresh and used electrodes (after cell was dismantled) by scraping off the electrode mass from the current collector in an argon-filled glove box with water and oxygen contents in the range 2–5 and 5–10 ppm, respectively.

The batteries were dismantled using an electrical circular saw to remove the laser-welded cap, allowing battery core (jelly-roll, JR) to be easily removed from the can. This operation was carried out in a dry room with controlled dew point (−45 °C) and water (50 ppm) to avoid short circuit. After the dissection of the prismatic cell, the jelly-roll consisting of negative electrode, positive electrode, separator, and residue of the electrolyte was immediately transferred to a glove box with a desiccator. The electrodes acquired in this way were neither washed nor dried.

Overcharge tests were carried out in a chamber with a current–voltage tester and temperature-control sensor. These tests were performed galvanostatically on prismatic cells of 720-mA h capacity and without positive temperature coefficient design to allow high-current charge capability. The overcharge test conditions were carried out at 1, 2, and 3 C, with a compliance voltage of 12, 9, and 6 V, respectively (difference in voltage is due to different testing standards applied in our tests).

"Soft" overcharge was carried out at 1 C constant current and a fixed voltage of 4.4, 4.6, and 5.0 V to simulate a malfunctioned charger. In other words, the subsequent charge step was terminated when cells reached 118, 150, and 200% of their discharged capacity (Table 1). After each charge step, cells were carefully dismantled and unwound. Current–voltage–temperature data were recorded every 5 s during overcharge.

## Results and discussion

### Overcharge at 1 C/12 V, 2 C/9 V, and 3 C/6 V

Taking into account different battery test standards used in industry and customer requests, we have studied three kinds of overcharge conditions, i.e., 1 C/12 V, 2 C/9 V, and 3 C/6 V. All tested cells ignited and burst after the rapid cell surface temperature increase. Figure 1 shows overcharge test result for (a) 1 C/12 V and (b) 3 C/6 V conditions.

In fact, every cell in each series of experiment has a different behavior, i.e., maximum cell temperature may have some difference for each single cell because of slightly different assemblage and cell quality.

Average data for each test set are shown in Fig. 2. From the figure, it is seen that as soon as cell voltage is over 5 V, the slope of the cell surface temperature increases significantly and thermal runaway and explosion soon follow.

Overcharge profiles give general information about the cell behavior (cell surface temperature and voltage) at different C rates. For a better understanding of the overcharge process, we have focused on the temperature range from room temperature to 100 °C (Fig. 3). There are two main segments on the temperature profile. In the first segment (from A to B with the temperature range from 25 °C (1 C/12 V) to 40 °C (3 C/6 V)), the temperature is approximately constant although the duration of this segment is different for different experiments (75 min for 1 C/12 V, 35 min for 2 C/9 V, and 25 min for 3 C/6 V). The second segment (from B to C with the temperature range from 40 to >100 °C) is the beginning of thermal runaway and is characterized by almost straight lines with steep slopes for all test conditions. The temperature increase for all samples in the segment A–B is the same (overcharge time—15 min as a check point) and is equal to 6 °C. However, the second segment (B–C) shows much difference between samples. In Fig. 3, we find that temperature rates (°C/min) for each sample are quite different in the segment B–C with linearly increasing temperature (from 40 to 80 °C). We find it is 4.2 °C/min (1 C/12 V), 12 °C/min (2 C/9 V), and 15 °C/min (3 C/6 V). It is interesting to note that an increase in current rate from 1 to 2 C will increase the temperature rate by three times but an increase of 1 to 3 C increases the temperature rate by less than four times. The sharp temperature slope (B–C in Fig. 3) corresponds to a voltage plateau in the range of 5–5.1 V ending with a short drop to 4.8 V in the temperature range from 70 to 80 °C and corresponding to the PE separator melting.

**Table 1** "Soft" overcharges steps for the 720-mA h Li-ion cell

| SOC (% of mA h) | Cell voltage (V) | Cell capacity (mA h) |
|---|---|---|
| 118 | 4.4 | 876 |
| 150 | 4.6 | 1,080 |
| 200 | 5.0 | 1,440 |

Figure 4 shows a heat output profile (calculations based on experimental data and Eq. 1) generated inside the cell for the whole overcharge process until cell explosion. All three profiles are quite straight lines with slightly different slopes (for example, 3 C/6 V is from 8 to 11 J). The behavior is similar to the temperature profile (Fig. 3) at the beginning of the overcharge test (15-min check point on Fig. 3, a–b). Heat output (electrical power) generated by the applied current does not vary its behavior like the cell surface temperature but simply increases proportionally with the current rate.

$$Q = I^2R = V^2/R(\mathrm{J/s}), \tag{1}$$

where $I$—current, $R$—cell resistance, and $V$—cell voltage.

This shows a clear relationship between the cell surface temperature (a–b, Fig. 3) and C rate of overcharge, i.e., the initial heat generation may be contributed mainly to the current value applied to the battery but not chemical reactions at least until cell voltage reaches some critical value. In other words, the A–B plateau (Fig. 3) where the cell is overcharged from 80% to 200% retains an almost constant surface temperature because of heat generation and dissipation by the applied current as well as endothermic $LiCoO_2$ deintercalation. It was shown by R.A. Leising et al. [14] that the internal resistance of the cell is not related to the current until the cell reaches 80–90% of charge (which is equivalent to 150% in our test).

This means that an increase of the cell internal resistance (1) due to electrolyte oxidation and decomposition of freshly deposited Li-ion anode surface and (2) due to high

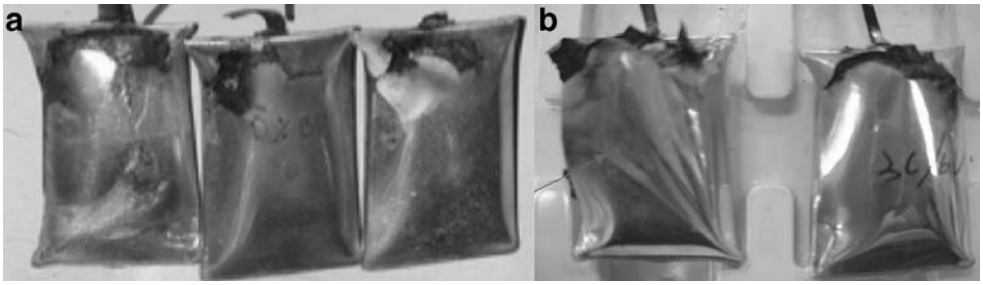


**Fig. 1** Li-ion cell (720 mA h) photographs after overcharge tests: 1 C/12 V (**a**) and 3 C/6 V (**b**)

delithiation of the cathode ($Li_xCoO_2$, $x<0.5$) is not the main factor in cell thermal runaway.

Another way to analyze overcharge data is shown in Fig. 5, the voltage profile for the overcharge test vs. time. Test data is extracted from Fig. 2 for every 5-°C temperature change resulting in Fig. 5. It is clear that there are several plateaus of cell voltage change during overcharge at 1, 2, and 3 C, respectively. These plateaus lie in the voltage range between 4.4 and 5.1 V and the change between the plateaus is step like. Note that the time scale in this case is not linear.

The voltage profile at 1 C/12 V conditions has three steps after the voltage reaches 4.4 V: A, B1, and C1. A ranges from 4.35 to 4.5 V, B is from 4.5 to 4.8 V, and C is between 4.9 and 5.1 V. Level A starts at 4.35 V 25 min after initiation of overcharge testing with an initial temperature of 24 °C (30% of overcharge capacity). It continues for 10 min at constant temperature 23–24 °C. B1 is from 4.5 to 4.8 V for the next 30 min while the temperature of the cell surface only increases to 25 °C. The last plateau C1 (4.9–5.1 V) continues for 19 min and the temperature increases almost linearly from 35 to 80 °C for 11 min. After the voltage drops to 0 V, the cell explodes (205.6% of overcharge capacity).

The cell with overcharge conditions (2 C/9 V) shows only two voltage plateaus. B2, from 4.5 to 4.9 V, continues for 13 min (from 15 to 28 min of overcharge) at constant temperature 28 °C. In the C2 plateau, the cell reached 5.1 V after 38 min of overcharge testing with 181% of overcharged capacity and then exploded at 43 min with 203% of overcharge capacity.

Overcharge at 3 C/6 V shows a voltage increase from 4.4 to 5 V in only 2 min. The cell reached 4.4 V 8 min after overcharge initiation. The cell surface temperature rose from 23 to 32 °C while the voltage was an almost constant 4.4 V. After the cell reached 4.5 V, the voltage slope rose very quickly to 5.01 V in 2 min followed by another voltage plateau of 5.1 to 5.0 V (C3) for 10 min until the cell voltage jumped to almost 6 V for less than 30 s and the cell surface temperature reached 90 °C. This happened after 28 min of overcharge testing and it corresponds to about 201.5% of overcharge capacity.

The last part of each C plateau clearly shows the duration and rate of separator melting as a function of voltage drop vs. time. It is seen that even for 1 C of overcharge rate the duration of the separator softening is only 8 min with a temperature increase rate of 4.2 °C/min. Under these conditions, thermal runaway cannot be averted by a current shutdown.

Another interesting example is an overcharge test of a cell with a capacity downgraded to 600 mA h. This was done with the same cell chemistry as the 720-mA h samples but with different dimensions (033450) of the Al can, i.e., 1 mm thinner to fit 600-mA h jelly-roll size. In Fig. 6, there are two overcharge profiles for 600 and 720-mA h cells at 1

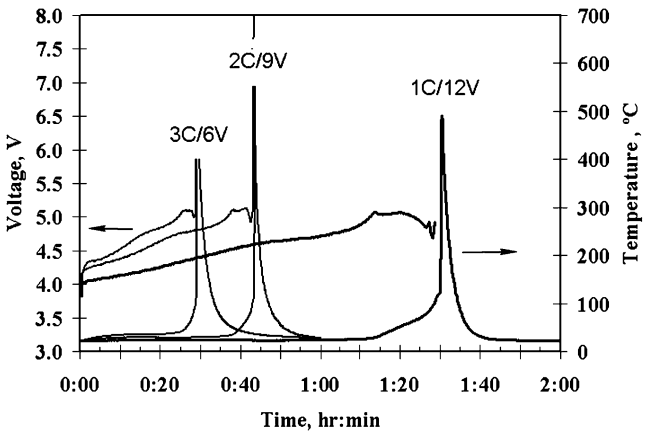


**Fig. 2** Overcharge test of Li-ion cell 720 mA h at 1 C/12 V, 2 C/9 V, and 3 C/6 V

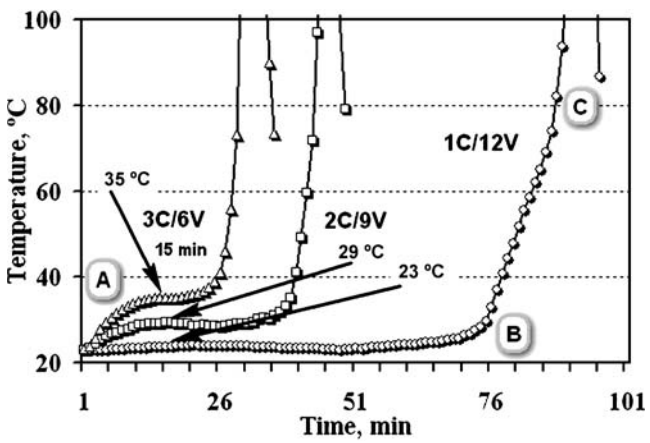


**Fig. 3** Cell surface temperature vs. time of overcharge and C rate

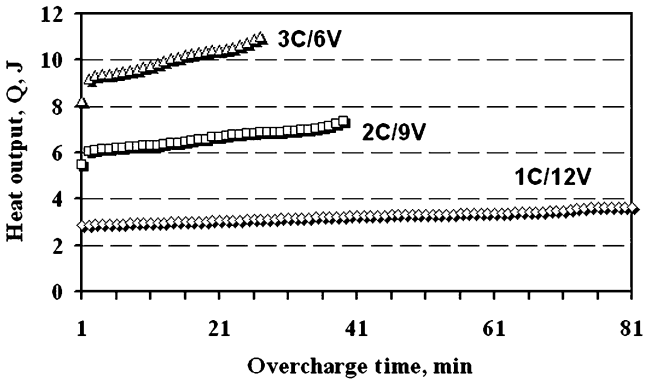


**Fig. 4** Heat output generation at different overcharge current rates calculated by Eq. 1 and experimental data (from 3.8 to 5.05 V)

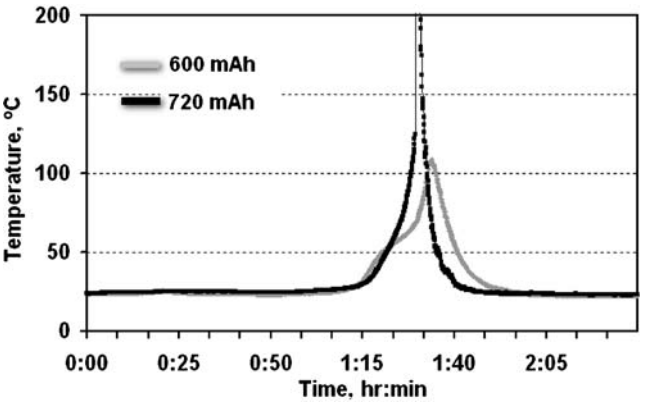


**Fig. 6** Overcharge test (1 C/12 V) of the commercial 033450 (600 mA h) and 043450 (720 mA h) cells

C/12 V conditions. The 600-mA h cell reaches the overcharge temperature even earlier than the 720-mA h cell and has a small shoulder at 50 °C (temperature rate from 40 to 80 °C is 2.8 °C/min). The maximum of the cell surface temperature was 105 °C, which quickly dropped to room temperature. The maximum voltage for the 600-mA h cell was 5.24 V and pressure rupture occurs. In the case of the 720-mA h cell, it attains a much higher temperature and ignites 5 min earlier than the 600 mA h. The temperature rose at the constant rate of 4.4 °C/min (from 40 to 80 °C).

The different behavior of cells with the same chemistry but different capacity and energy density may reveal some reasons to be concerned about safety. Although the highest surface temperature for 600-mA h cells is only 105 °C, the inside of the cell may reach more than 150 °C. When the cell temperature is higher than 150 °C, it could lead to SEI breakdown, electrolyte decomposition, and PE separator melting. However, there is no bursting or ignition observed in the test. Therefore, one reason for the safe behavior of the 600-mA h cell is the heat generation and heat dissipation rates. Another reason is the time taken for pressure rupture to open. In the case of the 720-mA h cell, the pressure rupture opened and the cell simultaneously burst and immediately caught fire. This was due to the safety vent and/or pressure rupture not working properly. It is difficult to design and optimize the safety vent operation conditions for an Al can as it is quite soft compared to iron-based cans.

Another factor that may have some influence on overcharge behavior is the concentration of Li salt ($LiPF_6$) in the electrolyte system. An increase in Li salt concentration of 0.15 M will delay thermal runaway by 18 min (105 °C) with a maximum voltage of 5.24 V for 1.1-M and 5.1 V for 1.25-M samples. However, this does not make the cell safer (Fig. 7).

These experimental results show that an increase in the C rate will raise the cell temperature to 23, 29, and 35 °C at current rates 1, 2, and 3 C, respectively, and this is mainly due to the heat generation by the current and the cell's ability to dissipate it. A detailed graphical presentation of the overcharge test data (Fig. 5) shows obvious stepwise voltage changes in the range of 4.4 to 5.1 V which may

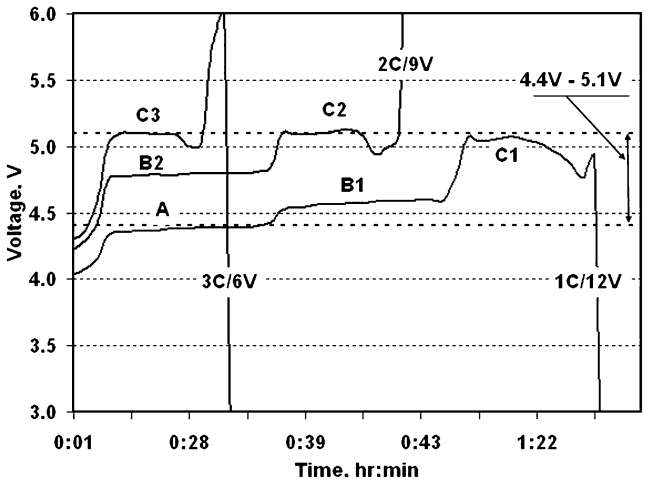


**Fig. 5** Extracted data for voltage change during overcharge test (Fig. 14) of Li-ion cell 720 mA h at 1 C/12 V, 2 C/9 V, and 3 C/6 V (graph re-plotted for every 5 °C change)

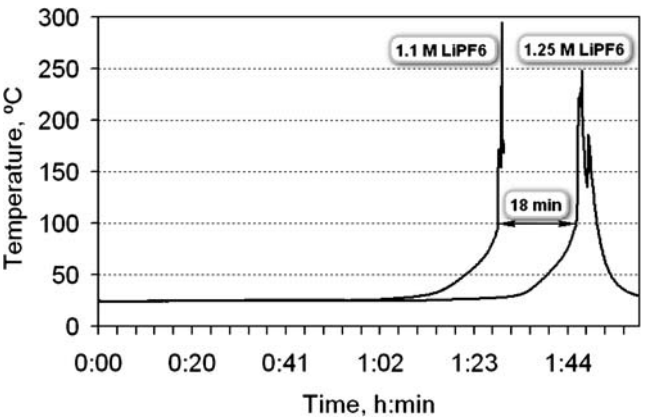


**Fig. 7** Overcharge test (1 C/12 V) of the 720-mA h cell with 1.1- and 1.2-M $LiPF_6$ electrolyte

indicate the different chemical processes occurring in the cells and help to determine the kinetics.

However, cell design and can construction could improve Li-ion battery safety significantly. A fast safety vent opening may stimulate overheating and explosion by the following mechanism. After the vent (or pressure-release rupture) is opened, the gas accumulating inside the cell will be released. After that, atmospheric air (with fresh oxygen and moisture) will enter the battery and react with the freshly plated Li metal and electrolyte, causing explosion and ignition.

## "Soft" overcharge

For a better understanding of the Li-ion cell failure mechanism at overcharge, the "soft" overcharge technique described in the "Materials and methods" section has been applied. A typical voltage–temperature profile of the Li-ion cells (720 mA h) charged to 5.6 V at constant current of 480 mA is presented in Fig. 8. Normally, cells will not reveal any change in shape until the voltage exceeds 4.8 V. The maximum voltage reached was 5.15 V, which then slowly dropped to 4.9 V while the temperature continued to rise to 85 °C (2 °C/min). If the temperature difference inside and outside the cell, which is about 60 °C [14], is taken into account, the shutdown of the polyethylene separator will start at about 70 °C (78 °C in this experiment). At this temperature, the voltage suddenly dropped to 4 V which is possibly due to separator pores closing as a result of polyethylene softening. This is true for the case of a low charge rate (<0.6 C) when cell temperature rises relatively slowly and the polymer separator melting rate is equal or close to the cell temperature rate. Another important condition for a polyethylene-based separator with a shutdown mechanism is uniformity of heating and also relative rates of heat removal and heat generation. We can assume that cell self-heating has inertness and cannot be stopped immediately after a certain point. Also, the temperature inside the JR is higher than temperatures close to the can wall. Another assumption is that the polymer separator shutdown mechanism has a certain rate and kinetic behavior of polymer softening and melting which is strongly related to (1) polymer material (molecular mass, porosity, etc.), (2) cell design or configuration (prismatic or cylindrical, intrinsic pressure), and chemistry. Tobishima and Yamaki [15] reported that low charging rates (<C/5) do not result in thermal runaway, while higher rates did. They conclude that when a cell cannot transfer heat to its environment at a rate equal to or higher than the rate of heat generation, it will undergo thermal runaway. But, in fact, there are many factors which are as important as charging rates. These include positive and negative material properties and nature, such as particle size, state of charge (SOC), electrolyte composition (Li salt concentration and its type and additives), separator characteristics (material base, pore size, and thickness), and quality of cell can (Al, stainless steel, and can wall thickness).

To find out how seriously the inner environment of the battery will degrade during continuous abuse conditions (i.e., overcharge), we performed "soft" overcharge tests at different conditions until cell explosion. Afterwards, test cells were carefully dismantled and cathode, anode, and separator materials were examined by visual observation as well as by DSC tests.

Figure 9 shows combined profiles of voltage and temperature as a function of time for three kinds of "soft" overcharge test conditions.

When the jelly-roll was unwound from the prismatic cell after the "soft" overcharge test (at 4.6 V with 150% SOC), the cathode electrode remained without notable visual changes. Strong Li metal plating and electrolyte decomposition appear on the anode electrode surface. After a few seconds of exposure to air, the anode surface changed to a white-light brown color (LiOH, $Li_2CO_3$, $(CH_2OCO_2Li)_2$). The separator surface has some residue (spots) on the anode side and small particles (like ash) on the folding parts and tab areas.

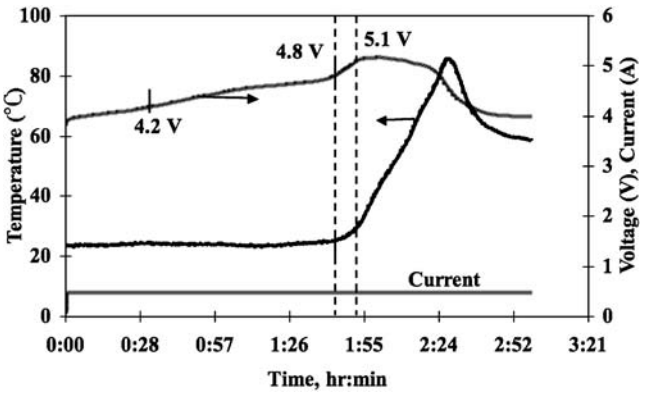


**Fig. 8** Typical voltage–temperature curve of Li-ion cells (720 mA h) during "soft" overcharge test at CC=500 mA to 5.6 V cutoff voltage

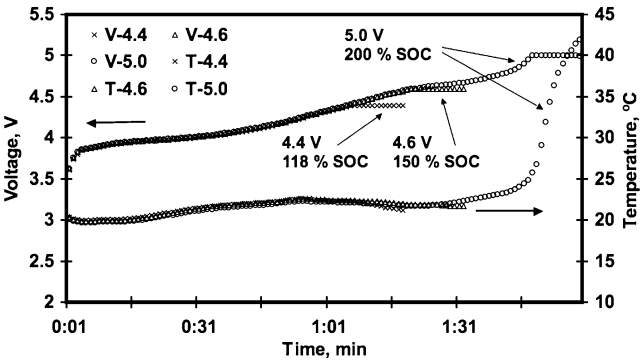


**Fig. 9** Typical voltage–temperature curve of 720-mA h Li-ion cells during "soft" overcharged test to 4.4, 4.6, and 5.0 V cutoff voltages at 1 C charge rate

A very different situation is observed for cells with SOC= 200% (overcharge to voltage 5 V). The cathode electrode almost separates from the current collector (Al foil). The anode electrode looks vulcanized and is separated from the current collector (Cu foil). The separator surfaces are blocked by the anode electrode film, which possibly penetrates the pores.

Heavy delamination of the electrode material from the current collector (either anode or cathode) is a result of foil surface oxidation due to moisture and oxygen released from electrolyte decomposition. The following chemical reactions may take place under soft overcharge conditions. During SEI formation and electrolyte decomposition, methane and alkyl radicals may be released [16]. With continuous overcharge, oxygen may be released from either electrolyte decomposition at high voltage or from the cathode crystal structure. At high pressure, methane forms formaldehyde (HCHO or $H_2CO$) which transforms to the formyl radical (HCO), which then forms carbon monoxide (CO) as follows:

$$CH_4 + O_2 -> CO + H_2 + H_2O, \quad \Delta H = -891\ \text{kJ} \qquad (2)$$

Following oxidative pyrolysis, the $H_2$ oxidizes, forming $H_2O$ and releasing heat. This occurs very quickly (less than a millisecond).

$$2H_2 + O_2 -> 2H_2O, \quad \Delta H = \text{exo} \qquad (3)$$

Then, the CO oxidizes forming $CO_2$ and releasing more heat over a few to several milliseconds.

$$2CO + O_2 -> 2CO_2, \quad \Delta H = \text{exo} \qquad (4)$$

Released heat from these reactions and heat from the reaction of the water with freshly plated Li will increase the cell external temperature dramatically in a few seconds.

Another phenomenon in the Li-ion battery at overcharge was found. The scanning electron microscopy image of the PE separator surface (anode side) after the soft overcharge test shows dendrite-like formations (Fig. 10). We suggest that this may be the result of the conducting material being continuously removed from the cathode through the separator film. Solvated Li ions bring conducting ash and decomposed electrolyte (such as $Li_2CO_3$, FH) and cathode material particles through the separator to the anode side. Because the separator film has a certain porosity, tortuosity, and pore size, the migration will slow down inside the separator. This will create such effects as dendrites growing inside the separator and on the separator surface (anode side). Elemental analysis confirms that most of the composition of such dendrites is conducting (Table 2). It can be assumed (according to separator surface appearance) that such dendrite growth will be located in certain areas. This may depend on the distance between the anode and the separator, consistency in pore size and/or porosity, cathode material quality, and so on. However, it will generate areas where soft shorting and local overheating may occur sooner than average. The number and composition of dendrites depend on (1) the separator material quality such as polyolefin molecular weight, thickness, porosity, and tortuosity, (2) the cathode material composition, and (3) the cell design. In addition, the kinetics of overcharge and failure mechanism of the cell during overcharge may vary.

Alternating current (AC) impedance (at 1 kHz) and cell thickness (volume expansion) have been examined during the "soft" overcharge test. As seen in Fig. 11, much of the notable volume expansion and impedance increase start after the cell reaches 4.4 V. Slopes of the volume expansion and AC impedance are very similar for both phases of overcharge at 4.2–4.4 and 4.4–5.0 V.

After each step of "soft" overcharge testing, electrical impedance spectroscopy test was performed at $E$=4.4 and 4.6 V (Fig. 12) in the frequency range of 100 kHz to 0.1 Hz. A Nyquist plot of the cell after the formation step is given as a reference and marked as «no overcharge—4.2 V». The inset details are the high frequency regime. The Nyquist plot shows a dramatic increase in resistance for the 4.6 and 5.0 V test. It was found that the AC impedance spectra for the cell at 4.2 and 4.4 V consisted of two suppressed arcs in the high frequency range and a narrow line inclined at constant angle to the real axis (Warburg impedance) in the low frequency

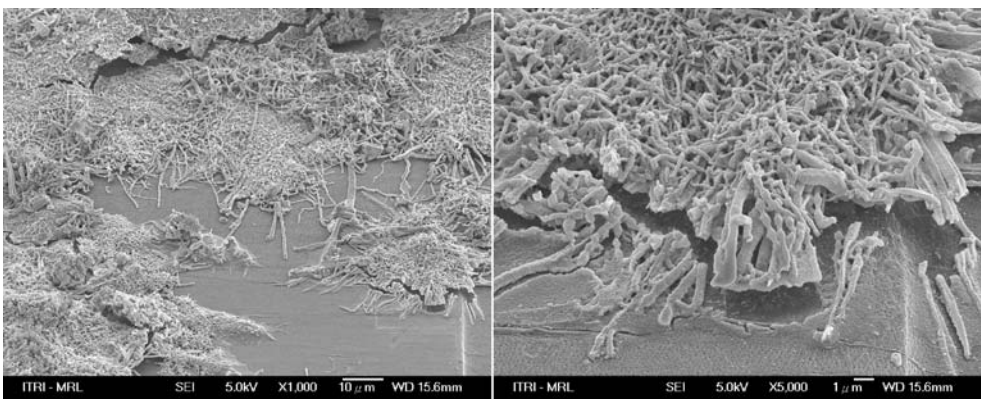


**Fig. 10** SEM of the separator PP/PE/PP surface (anode side), after soft overcharge (*left*—magnification ×1,000); SEM of the separator PP/PE/PP surface (anode side), after soft overcharge (*right*—magnification ×5,000)

**Table 2** EDS data of the dendrites on separator surface after overcharge test

| Element | C | O | F | Si | P | S | Co | Cu | Total |
|---|---|---|---|---|---|---|---|---|---|
| Weight, % | 20.33 | 35.9 | 31.21 | 0.41 | 2.62 | 1.34 | 5.75 | 2.43 | 100 |
| Atomic, % | 28.91 | 38.31 | 28.05 | 0.25 | 1.44 | 0.71 | 1.67 | 0.65 | |

range. However, for cells overcharged to 4.6 and 5.0 V, the Warburg impedance did not appear.

It is generally known [17, 18] that the potential-invariant first arc is mainly caused by the formation of a passive film on the electrode surface, i.e., solid electrolyte interface film. The second middle-frequency semicircle is probably due to a charge-transfer reaction at the interface, which depends significantly on the electrode potential. In addition, the Warburg impedance is associated with the diffusion of lithium in the electrode.

As seen from Fig. 12, when the cell is overcharged over 4.5 V, the second semicircle enlarges dramatically, which may be associated with abnormal SEI thickness growth and very little Li diffusion (Warburg impedance).

## Thermal stability of electrodes at overcharge (DSC)

*Anode* Three types of overcharged anode electrodes are presented in Fig. 13. Each shows two main peaks in the region of 120–140 and 300–320 °C; the first is attributed to SEI-layer breakdown and the second one is mainly due to heat generation as a result of reactions between plated lithium metal, $Li_xC_6$, and PVDF. It has been suggested [3, 19, 20] that the exothermic peak at 120–140 °C is due to metastable components such as $ROCO_2Li$ species present at the interface of the anode electrode (reduction products of EC and EMC/DMC) reacting with traces of water and hydrofluoric acid to form $CO_2$, which is immediately reduced to $Li_2CO_3$.

In the case of the samples overcharged to 4.6 V ($\Delta H_2$) and 5.0 V ($\Delta H_3$), the exothermic peaks at 120–140 °C (Fig. 13) are almost two times larger (but the intensity is the same, except for the 5.0 V sample which has slightly lower intensity) than the peak for the sample overcharged to 4.4 V ($\Delta H_1$). This is a result of a higher concentration of reduction products from SEI and the electrolyte produced at different states of overcharge.

$$\left(\Delta H_2 \approx \Delta H_3; \Delta H_{2,3} \gg \Delta H_1; \Delta H_{2,3} \approx 1/2\Delta H_1\right)$$

*Cathode* DSC scans of the cathode materials (Fig. 14; Table 3) recovered from the prismatic cell overcharged at 4.4 V (118% SOC) and 4.6 V (150 and 200% SOC) show two main peaks in the region of 150–250 and 300–400 °C. These heat generation peaks are attributed to electrode material decomposition following oxygen liberation. Dahn et al. [5] have shown that, above some critical temperature, cathode materials such as $Li_xNiO_2$, $Li_xCoO_2$, or $Li_xMn_2O_4$ are unstable and liberate oxygen into the electrolyte which, when heated above its flash point, react violently. The amount of oxygen released on heating increases with a decrease in the $x$ value. For $Li_xCoO_2$, the lower critical value of $x$ is near 0.5. In our experiment, the first exothermic peak has a maximum temperature of about

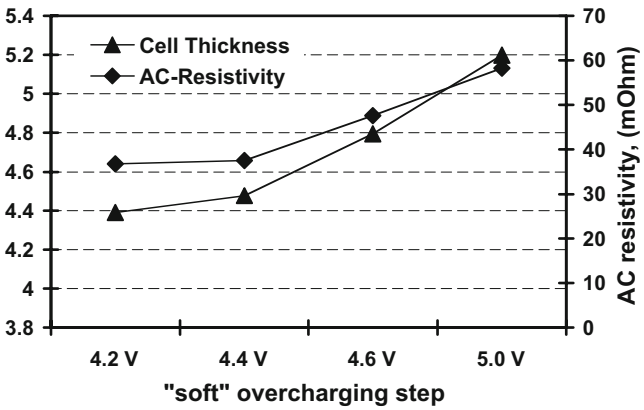


**Fig. 11** Cell thickness and AC resistance as a function of "soft" overcharge at 1 C rate of 720-mA h Li-ion cell

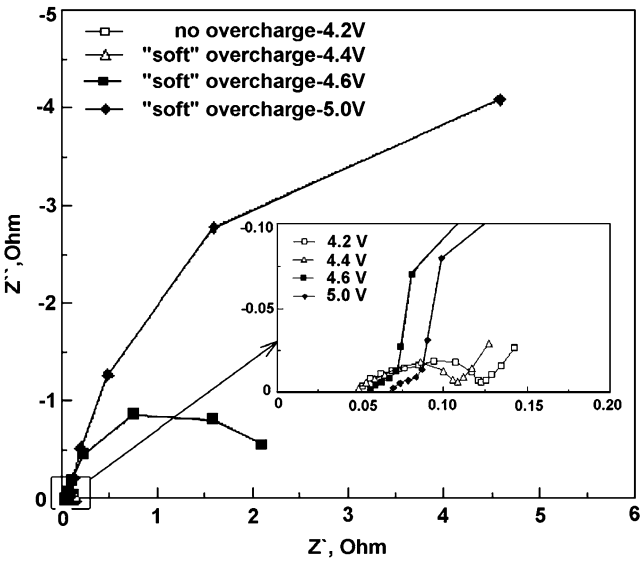


**Fig. 12** Nyquist plot of "soft" overcharged 720-mA h Li-ion cells; the *inset* shows a magnified view of the high frequency part

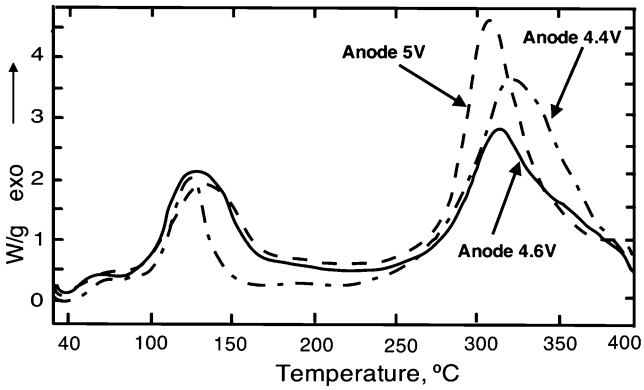


**Fig. 13** DSC profiles of anode electrode from 720-mA h Li-ion cell after "soft" overcharge to 4.4, 4.6, and 5.0 V, OCV=4.4 and 4.6 V

225 °C (4.4-V sample) which appears to be much wider than what is usually observed in DSC results for cathode materials. It is a result of $Li_xCoO_2$ decomposition (with lower $x$—temperature shifts to lower value), which accelerates at lower temperatures, and the reaction of some electrolyte solvent residue with the remaining $Li^+$. Maleki et al. [4] showed by X-ray diffraction analysis that the cathode material of the cell (open circuit voltage (OCV)= 4.15 V) restructures before initiating the major decomposition or heat generation step above 235 °C. On heating to temperatures above 245 °C, delithiated $Li_xCoO_2$ decomposes to form a layered structure of $LiCoO_2$. For the sample with SOC=200% (5.0 V), the low temperature peak divides into two (200 and 260 °C) which is probably the result of more serious structural changes in $Li_xCoO_2$. The onset point shifts to lower temperatures as follows: 150 °C (4.4 V), 125 °C (4.6 V), and 90 °C (5.0 V).

Comparing DSC data for both anode and cathode materials, we can allocate two temperature regimes: low temperature (LT; <250 °C) and high temperature (HT; >300 °C).

For the cathode material, increasing the cutoff charged voltage from 4.4 to 5.0 V shifts temperature maxima from 235 to 200 °C and from 345 to 320 °C in the LT and HT regimes,

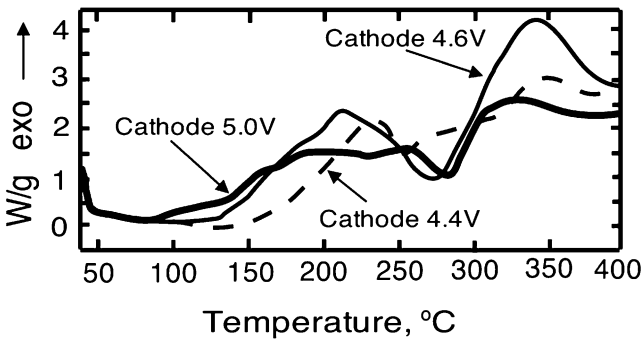


**Fig. 14** DSC profiles of cathode electrode from 720-mA h Li-ion cell after "soft" overcharge to 4.4, 4.6, and 5.0 V, OCV=4.4 and 4.6 V

**Table 3** Maximum DCS temperatures of cathode and anode materials recovered from cells overcharged to 4.4, 4.6, and 5.0 V

| | Low-temperature area, <250 °C | | High-temperature area, >250 °C | |
|---|---|---|---|---|
| | Cathode (LT) | Anode (LT) | Cathode (HT) | Anode (HT) |
| 4.4 V | 235 | 120 | 345 | 320 |
| 4.6 V | 210 | 125 | 340 | 315 |
| 5.0 V | 200 | 130 | 320 | 310 |

respectively. This can be explained by the above-mentioned changes in the $LiCoO_2$ structure. Delithiation of $Li_xCoO_2$ at $x<0.5$ transforms it into a metastable state: $Co^{3+} \rightarrow Co^{4+}$. The lower the value of $x$, the easier it is for $Li_xCoO_2$ to release $O_2$ and immediately react with the electrolyte.

The anode material shows the opposite behavior, i.e., in the LT regime, the maximum temperature shifts from 120 to 130 °C when the overcharged voltage increases from 4.4 to 5.0 V. This is probably due to growth of SEI layer and side reactions. In the HT regime, the anode material behavior is similar to the cathode material, i.e., the maximum temperature decreases from 320 to 310 °C.

As seen from the DSC study of the "soft" overcharged anode and cathode materials, most major heat generation processes occur after the temperature reached more than 200 °C, which is far from the typical battery failure starting point of 80 °C on the cell surface or about 130 °C inside the cell surface. The only exception is the SEI-layer breakdown peak at about 120 °C, which is very low (about 200 J/g [21]); however, it may trigger other processes such as methane gas burning. It can be concluded that the amount of heat generated during the overcharge process (thermal runaway stage) is much less dependent on the nature of the material than was previously supposed.

## Conclusions

In this study, we described a "soft" overcharge technique, which is a part of a complex study on Li-ion battery safety. This technique allows us to trace the overcharge process gradually and find the stage(s) when cell conditions become most critical and irreversible. It also lets us look at the overcharge process from a different point of view.

It was found that a Li-ion battery with $Li_xCoO_2/Li_yC_6$ chemistry may have a dramatic change at 150% of overcharged capacity. The PE separator of 16-μm thickness did not follow appropriate shutdown mechanisms at current rate 1 C and all cells exploded. However, when the current rate was less than 0.7 C and the cell surface temperature rate was less than 3 °C/min, the separator did follow some protection mechanism but did not cut off the current completely.

Destruction of the anode and cathode starts when the cell reaches 5 V (i.e., 200% of overcharged capacity).

The most interesting observation was made when the separator was recovered from the overcharged cell. It was found that the separator surface (anode contacted side) had some growth, which mainly consisted of cathode micro particles and products of electrolyte decomposition reactions. This suggests that one of the main factors of the cell failure at overcharge might be micro-shorting initiated by such electro-conducting growth penetrating through the separator with solvated Li ions. In combination with a high energy density design, this will obviously provoke local micro-shorting and side reactions with the electrolyte and gaseous by-products (such as methane), initiating a chain reaction leading to thermal runaway. On the other hand (if considering over-charge tests to be accelerated cycle life tests), prolonged cycling will generate the same growth phenomena on a thin separator and cause micro-shorting, which will cause slow overheating and finally explosion. Our tests show that the assertion that $LiCoO_2$ and its unstable structure are the main factors for Li-ion battery failure at overcharge is not necessarily a fact and much heat is generated well after the initiation of battery thermal runaway.

Cell design, separator quality and properties, and can construction could improve Li-ion battery safety significantly. Fast safety vent opening may stimulate overheating and explosion. Therefore, construction of the vent to release pressure from the battery slowly (before the critical value is reached and preventing fresh air to get into the cell) is extremely important. Soft packs (pouch cell design) are a good solution for some applications in terms of safety.

## References


1. Reimers JN, Dahn JR (1992) J Electrochem Soc 139:2091
2. Maleki H, Hallaj SA, Selman JR, Dinwiddie RB, Wang H (1999) J Electrochem Soc 146:947
3. Du Pasquier A, Disma F, Bowmer T, Gozdz AS, Amatucci GG, Tarascon J-M (1998) J Electrochem Soc 145:472
4. Maleki H, Deng G, Anani A, Howard J (1999) J Electrochem Soc 146:3224
5. Dahn JR, Fuller EW, Obrovac M, von Sacken U (1994) Solid State Ionics 69:12
6. Cho J (2004) J Power Sources 126:186
7. Kim J, Noh M, Cho J (2006) J Power Sources 153:345
8. Cho J, Kim T-G, Kim C, Lee J-G, Kim Y-W, Park B (2005) J Power Sources 146:58
9. Xiao L, Ai X, Cao Y, Yang H (2004) Electrochim Acta 49:4189
10. Moshuchak LM, Bulinski M, Lamanna WM, Wang RL, Dahn JR (2007) Electrochem Comm 7:1497
11. Chen G, Thomas A, Karen E, Newman J, Richardson TJ (2005) Electrochim Acta 50:4666
12. Underwriters Laboratories (1995) A safety standard for lithium batteries, UL 1642, 3rd edn.
13. Japan Battery Association (1997) Guideline for the safety evaluation of secondary lithium cells. Tokyo, Japan
14. Leising RA, Palazzo MJ, Takeuchi ES, Takeuchi KJ (2001) J Electrochem Soc 148:A838
15. Tobishima S, Yamaki J (1999) J Power Sources 81–82:882
16. Kumai K, Miyashiro H, Kobayashi Y, Takei K, Ishikawa RI (1999) J Power Sources 81–82:715
17. Aurbach D, Gamolsky K, Markovsky B, Salitra G, Gofer Y, Heider U, Oesten R, Schmidt M (2000) J Electrochem Soc 147:1322
18. Hjelm AK, Lindbergh G (2002) Electrochim Acta 47:1747
19. Aurbach D, Zaban A, Gofer Y, Ein Ely Y, Weissman I, Chusid O, Abramson O (1995) J Power Sources 54:76
20. Aurbach D, Ein Eli Y, Markovsky B, Zaban A, Luski S, Carmeli Y, Yamin H (1995) J Electrochem Soc 142:2882
21. Zhang Z, Fouchard D, Rea JR (1998) J Power Sources 70:16